AJNR

A Novel Image Fusion Visualizes the Angioarchitecture of the Perforating Arteries in the Brain

Shigetoshi Shimizu, Hidenori Suzuki, Hiroaki Maki, Masayuki Maeda, Fumitaka Miya, Karim Benali, Yves Trousset and Waro Taki

AJNR Am J Neuroradiol 2003, 24 (10) 2011-2014
http://www.ajnr.org/content/24/10/2011

AJNR Am J Neuroradiol 24:2011–2014, November/December 2003

Technical Note

A Novel Image Fusion Visualizes the Angioarchitecture of the Perforating Arteries in the Brain

Shigetoshi Shimizu, Hidenori Suzuki, Hiroaki Maki, Masayuki Maeda, Fumitaka Miya, Karim Benali, Yves Trousset, and Waro Taki

Summary: We report a novel technique that fuses 3D digital subtraction angiograms and MR images. Image fusion was successfully performed within 20 minutes each in 11 consecutive cases. Our initial experience showed that this image fusion enabled clear and simultaneous visualization of perforating arteries and surrounding tissues. The relation between perforating arteries and normal brain or lesions was easily understood in a clinical setting by using this image fusion.

Three-dimensional digital subtraction angiography (3D DSA) is the best technique to provide anatomic details of vasculature (1–3). By contrast, MR images most clearly visualize intracranial tissues. Thus, fusion of 3D DSA and MR images may enable clear visualization of both the intracranial vasculature and tissues and may be useful for neurosurgeons and neuroradiologists to more easily understand their relation in a clinical setting. On the other hand, the perforating arteries, especially the recurrent artery of Heubner (RAH) and the lateral lenticulostriate artery (LSA), supply regions essential to neurologic functions and, therefore, their microsurgical anatomy has been aggressively studied mainly by using cadaveric dissections (4–6). Nonetheless, even with state-of-the-art imaging, it is still challenging to demonstrate them. The goal of this study was to evaluate a novel image fusion of 3D DSA and 3D MR images (3D DSA-MR fusion) and to visualize perforating arteries, in terms of the RAH and LSA, in brain tissue.

Technical Description

Subjects

Between September 2002 and February 2003, image fusion was performed in 11 consecutive patients (eight female and three male; mean age, 61.2 years; age range, 38–77 years) as a part of pre- or post-treatment evaluations for various intracranial diseases, including unruptured aneurysm (n = 4), brain tumor (n = 6), and arteriovenous malformation (n = 1). Appropriate informed consent was obtained from the patients or their relatives. No procedure-related morbidity or mortality occurred, and examination was well tolerated by all 11 patients.

3D DSA

All patients underwent 3D DSA under local anesthesia. The tip of a catheter was guided from the right radial artery and positioned in the common carotid or internal carotid artery (ICA). Standard 2D DSA was initially performed and thereafter, rotational angiography was performed as described elsewhere (1). The principle of 3D DSA was to reconstruct a high-spatial-resolution 3D image of the vasculature of the brain from a series of subtracted conventional radiographic images acquired during a rotation of a vascular C-arm (LCN+; GE Medical Systems, Milwaukee, WI) around the patient (1). For rotational angiography, a total of 24 or 27 mL of contrast agent (Iopromide 300 mgI/mL; Tanabe Seiyaku, Osaka, Japan) was injected at a rate of 4 or 4.5 mL/s. The images were immediately transferred to a workstation (Advantage Workstation 3.1p; GE Medical Systems) via a network. Image distortions were corrected as described elsewhere (1). The 3D DSA image was reconstructed in a 512 × 512 × 512 matrix, with an isotropic voxel size (0.3 mm when using a 22-cm field of view during acquisition). This high spatial resolution allowed precise visualization of small vessels such as perforating arteries. Reconstructed images including maximum intensity projection (MIP), surface shaded display, and volume rendering were made available. Processing was performed manually to optimize the display. All 3D images were stereoscopically arranged.

3D Spoiled Gradient Recalled (SPGR) MR Images

MR imaging was performed with a 1.5-T superconducting unit (Signa; GE Medical Systems) by using a standard quadrature head coil. The 3D SPGR images were obtained after intravenous injection of gadopentetate dimeglumine ([0.1 mmol/kg] Magnevist; Berlex, Montville, NJ). The imaging parameters were as follows: 30/3.1 (TR/TE), acquisition bandwidth of 15.6 kHz, a flip angle of 20°, a matrix of 256 × 192, and a field of view of 20 cm. The acquisition data were increased to a 512 × 384 matrix by using an interpolation technique. A total of 76 sections of 1-mm thickness were obtained, resulting in of 76 mm of overall vessel coverage. A slab was placed to include the distal ICA and the proximal vessels of the circle of Willis. The imaging time was 7 minutes 44 seconds.

3D DSA-MR Fusion

The 3D DSA and contrast-enhanced SPGR MR images were fused on the workstation by using the prototype image fusion software XR/MR Fusion (GE Medical Systems). This

Received May 23, 2003; accepted after revision June 22.

From the Departments of Neurosurgery (S.S., H.S., F.M., W.T.) and Radiology (H.M., M.M.), Mie University School of Medicine, Mie, Japan; and GE Medical Systems (K.B., T.Y.), Buc, France.

Part of this study was presented at the 26th Annual Meeting of the Japan Society for CNS Computed Imaging, Nagoya, February 7–8, 2003, and the 32nd Annual Meeting of the Japanese Society on Surgery for Cerebral Stroke, Tokyo, March 14–15, 2003.

Address correspondence to Hidenori Suzuki, MD, Department of Neurosurgery, Mie University School of Medicine, 2–174 Edobashi, Tsu, Mie 514-8507, Japan.

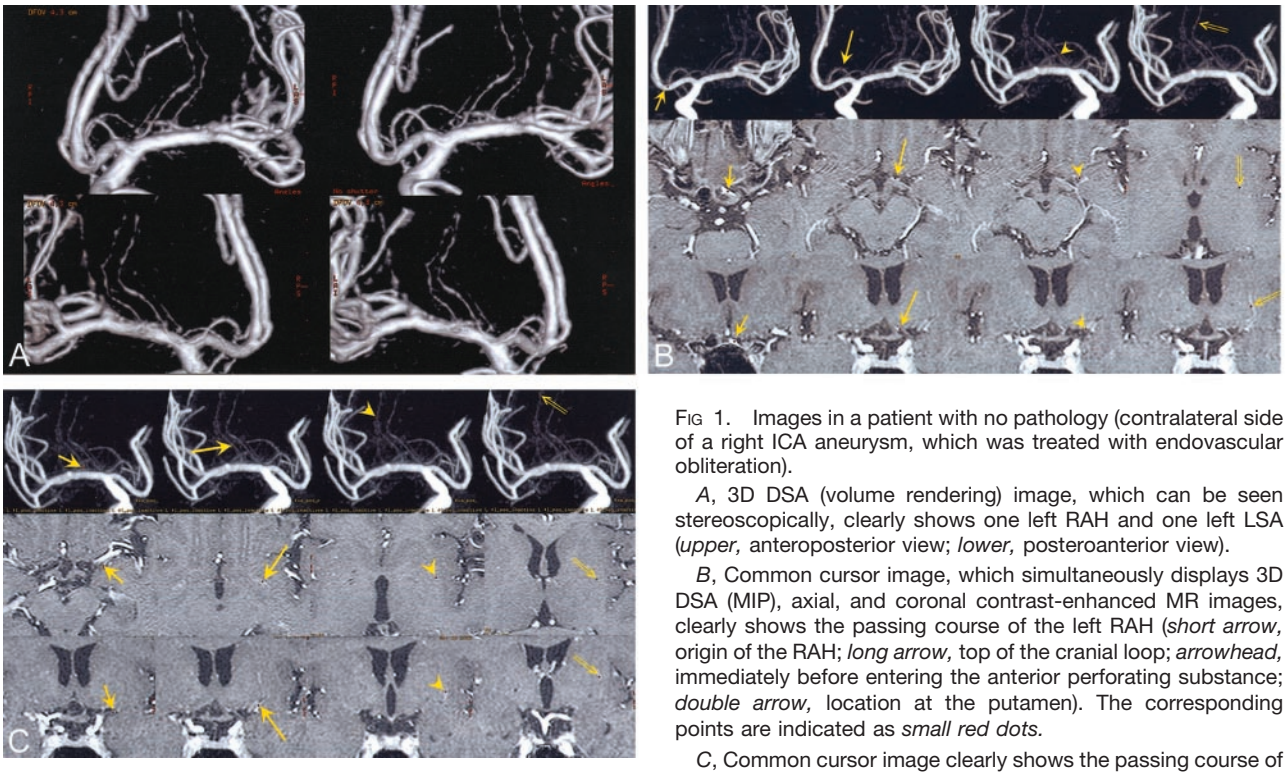

FIG 1. Images in a patient with no pathology (contralateral side of a right ICA aneurysm, which was treated with endovascular obliteration).

A, 3D DSA (volume rendering) image, which can be seen stereoscopically, clearly shows one left RAH and one left LSA (*upper,* anteroposterior view; *lower,* posteroanterior view).

B, Common cursor image, which simultaneously displays 3D DSA (MIP), axial, and coronal contrast-enhanced MR images, clearly shows the passing course of the left RAH (*short arrow,* origin of the RAH; *long arrow,* top of the cranial loop; *arrowhead,* immediately before entering the anterior perforating substance; *double arrow,* location at the putamen). The corresponding points are indicated as *small red dots.*

C, Common cursor image clearly shows the passing course of the left LSA (*short arrow,* location in the sylvian fissure; *long arrow,* location at the anterior perforating substance; *arrowhead* and *double arrow,* locations at the putamen). The corresponding points are indicated as *small red dots.*

prototype software was based on a new algorithm for automated registration of 3D DSA and MR images (7). The registration procedure started with manual designation of a predefined anatomic point in both modalities. For anterior circulation, this point might be, for instance, the origin of the middle cerebral artery, whereas for posterior circulation it might be the tip of the basilar tree. Registration between 3D DSA and MR images was then performed. This automatic registration could be seen as a search for rigid-motion transformation (rotation, translation, scaling) between the 3D DSA and MR models. Scaling could be derived from knowledge of the voxel sizes in both modalities and, therefore, only rotation and translation had to be estimated from the data. For this purpose, an original voxel-based registration technique was developed (7). The principle of voxel-based registration was to define a "similarity function" that characterized the similarity between the voxel densities in the two 3D volumes (3D DSA and MR) and to take as a solution to the registration problem the rotation and translation that would maximize this similarity function. In the method we used, the common anatomic point indicated by the user provided an initial estimate of the translation. Rotation was then estimated through a first maximization of the similarity function, and finally translation was re-estimated through a second maximization of the similarity function. This method was evaluated (7) against a stereotactic frame registration of a set of clinical data (nine patients). Maximum registration error was found to be less than 4 mm. The entire registration process took less than 30 seconds per case. When the process was completed, we validated and manually fine-tuned, if required, the registration identified by the software.

Image fusion was successfully performed within 20 minutes in all patients. This software provided several methods to display the fused 3D DSA and MR images. The method used in this study was called "common cursor." In this method, one 3D DSA image (MIP) and three cross-sectional MR images (axial, coronal, and sagittal) were displayed at the same time on the monitor. When clicking on any point on any of the four images, the software indicated automatically and in real time the corresponding points on all three other images. Using this method, we could evaluate the accuracy of the registration between the vessels in 3D DSA and the hyperintense areas in the three MR sections, which corresponded to vessels on contrast-enhanced SPGR MR images. Actually, the maximum registration error when aligning matching anatomic landmarks was less than 2 mm; this error became insignificant after re-registration. Common cursor images easily demonstrated which location of a perforating artery on 3D DSA images corresponded to a hyperintense spot or string on contrast-enhanced MR images, and vice versa. Common cursor images were also very useful for visualizing its passing course in brain tissue on three cross-sectional MR images by tracing a perforating artery on the MIP image; we used the stereoscopically arranged volume rendering images as a reference of the course of the perforating artery on 3D DSA.

Illustrative Cases

The Contralateral Side of an ICA Aneurysm

One RAH and one LSA were recognized on 3D DSA images (Fig 1A). The passing course of both arteries in brain tissues was demonstrated on common cursor images (Figs 1B and C). It was clearly shown that the RAH entered the anterior perforated substance just medial to the LSA. The RAH was clarified to supply the lateral part of the caudate head, and the LSA passed through the lateral part of the putamen.

Brain Tumor: Right Thalamic Malignant Lymphoma

One RAH and two LSAs were recognized on 3D DSA. The relation between these perforating arteries and a tumor were clearly shown on common cursor images (Fig 2).

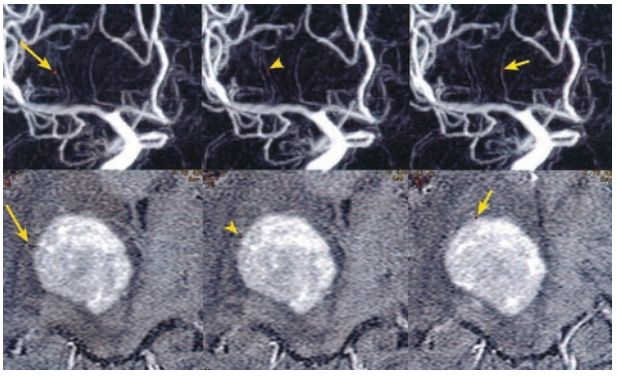

FIG 2. Common cursor image in a patient with a right thalamic malignant lymphoma. The image, which simultaneously displays 3D DSA (MIP) and axial contrast-enhanced MR images, clearly shows the relation between the tumor and two LSAs (*long arrow* and *arrowhead*) or one RAH (*short arrow*). The corresponding points are indicated as *small red dots.*

Discussion

The perforating arteries may be involved in various neurologic diseases. When neurosurgeons or interventional neuroradiologists plan their treatment, it is important to know whether the involved arteries supply the functionally important brain tissues. Neuroimaging of perforating arteries is still a challenging field, however, and has depended on DSA. The most sophisticated angiographic technique, 3D DSA, gives more precise and stereoscopic anatomic details of vasculature than previous angiographic techniques but provides no information about brain tissue (1–3). Although MR imaging shows good spatial resolution and an excellent contrast with the soft tissues of the brain, a detailed analysis of the vasculature of the brain cannot be performed. In this study, we presented a novel image fusion made by registration of 3D DSA to 3D MR images (DSA-MR fusion) and showed that this image was a unique and attractive technique able to visualize even the perforating arteries in brain tissue. DSA-MR fusion clearly showed the passing course and distribution of perforating arteries in brain tissue. In addition, DSA-MR fusion was very useful for identifying the perforating arteries involved in or surrounding various lesions and for visualizing the spatial relation between the perforating arteries and a lesion. Thus, DSA-MR fusion may enable pretreatment assessment of the functional risks associated with vascular injuries by the neurosurgical or the endovascular treatment.

Recently, image fusion techniques consisting of registering different kinds of images have been advanced in brain images (8, 9). The interest for image fusion comes from the idea that creating a fused image that combines two modalities may bring more information than analyzing these two modalities separately. Previous studies reported the combination of MR images with CT, intracranial echography, single photon emission CT, or positron emission tomography (8, 9). To our knowledge, however, no image fusion combining 3D MR images with 3D DSA, which gives information about both the intracranial soft tissues and vasculature, have been previously reported.

DSA-MR fusion can visualize any perforating artery visible on 3D DSA. 3D DSA cannot, however, visualize all perforating arteries. The vascular territory or size of a perforating artery is variable and reciprocal and depends on the degree of development of individual arteries (4–6). According to cadaveric dissections, one to three RAHs and two to 12 LSAs are recognized (4–6), but only one RAH and one or two trunks and four to eight branches of LSAs are most commonly visible on angiography (10). Although visualization of RAHs and LSAs has not been sufficiently investigated with 3D DSA, the image quality of 3D DSA may be degraded by some artifacts (1, 2). The causes of the degradation of the image quality include the following mechanisms: misregistration due to equipment vibration, relatively poor visualization of small vessels due to a slower injection rate of contrast medium, and the patient's motion artifact associated with a longer acquisition time (2). In this study, we adjusted the window levels of MIP images and the threshold levels of volume rendering images, selected contiguous objects, cut overlying structures, examined 3D DSA images from desired angles, and arranged 3D DSA images stereoscopically to optimize the display. As a result, 3D DSA visualized one to two RAHs and one to four LSAs, and the RAH was equivocal in only one case. The improved resolution of 3D DSA in the future may lead to visualization of a greater number of perforating arteries and contribute to our understanding of the clinical anatomy of perforating arteries by using DSA-MR fusion.

3D CT angiography (CTA) is undoubtedly a promising technique for demonstrating complicated 3D anatomy of vasculature, and the resolution of CTA is currently beginning to approach that of DSA. A recent study reported that 3D CTA demonstrated perforating arteries up to 1 mm in size (11). Because 3D CTA is relatively noninvasive, it may be worthwhile to try image fusion combining 3D MR images with 3D CTA, instead of 3D DSA.

The preferred MR acquisition for DSA-MR fusion is contrast-enhanced T1-weighted images, because the automatic setup is designed to work with contrast-enhanced T1-weighted images (7). This is because injection of gadolinium allows excellent contrast between vessels and surrounding soft tissues on MR images. Other types of MR acquisition can be used, but the automatic setup may not work. Registration and fusion are still possible, but users may need to do so manually (by designating three points in 3D DSA and MR images). In this study, 3D contrast-enhanced SPGR MR images were used as fused MR images. If other types of MR acquisition are used, DSA-MR fusion may provide important information other than the present findings; however, it remains an important area for further investigation.

DSA-MR fusion may have some image distortions, which include the distortions inherent in 3D DSA and MR images such as pincushion distortion and S distortion, and those associated with image fusion (1, 7,

12). These image distortions can be corrected as described in the Technical Description section. The vessels visible on 3D DSA are also visualized on 3D contrast-enhanced SPGR MR images, although MR images alone cannot precisely demonstrate which one is the RAH or the LSA. In the common cursor method, one 3D DSA image (MIP image) and three cross-sectional XR images are simultaneously shown, and the corresponding points on each image are identified on the workstation in real time. Thus, by using the common cursor, registration quality can be assessed by examining whether the point on the artery selected on the 3D DSA image is superimposed on the corresponding MR images, and its pathway along the artery can be tracked. If a significant registration error is encountered, it can be re-registered either manually or automatically. In this study, however, registration error was insignificant in all cases.

Conclusion

A novel image fusion technique, DSA-MR fusion, enabled clear visualization of the perforating arteries passing through the brain tissue. Using this image fusion, the relation between brain tissues or lesions and the vasculature, including individual perforating arteries, can be more easily and precisely understood than with 3D DSA and MR images separately.

Acknowledgments

We are grateful to Koichi Shibakusa (GE Yokogawa Medical Systems, Tokyo, Japan) for technical support and for assistance in preparing the manuscript.

References

1. Anxionnat R, Bracard S, Ducrocq X, et al. **Intracranial aneurysms: clinical value of 3D digital subtraction angiography in the therapeutic decision and endovascular treatment.** *Radiology* 2001;218: 799–808
2. Sugahara T, Korogi Y, Nakashima K, et al. **Comparison of 2D and 3D digital subtraction angiography in evaluation of intracranial aneurysms.** *AJNR Am J Neuroradiol* 2002;23:1545–1552
3. Hochmuth A, Spetzger U, Schumacher M. **Comparison of three-dimensional rotational angiography with digital subtraction angiography in the assessment of ruptured cerebral aneurysms.** *AJNR Am J Neuroradiol* 2002;23:1199–1205
4. Marinkovic S, Gibo H, Milisavljevic M, Cetkovic M. **Anatomic and clinical correlations of the lenticulostriate arteries.** *Clin Anat* 2001; 14:190–195
5. Gorczyca W, Mohr G. **Microvascular anatomy of Heubner's recurrent artery.** *Neurol Res* 1987;9:259–264
6. Rosner SS, Rhoton AL Jr, Ono M, Barry M. **Microsurgical anatomy of the anterior perforating arteries.** *J Neurosurg* 1984;61:468–485
7. Kerrien E, Levrier O, Anxionnat R, et al. **Automated registration of 3D X-ray angiography images to magnetic resonance images.** *Proc SPIE Med Imaging* 2001;4322:623–632
8. Julow J, Major T, Emri M, et al. **The application of image fusion in stereotactic brachytherapy of brain tumours.** *Acta Neurochir (Wien)* 2000;142:1253–1258
9. Stokking R, Zuiderveld KJ, Hulshoff Pol HE, et al. **Normal fusion for three-dimensional integrated visualization of SPECT and magnetic resonance brain images.** *J Nuc Med* 1997;38:624–629
10. Leeds NE. **The striate (lenticulostriate) arteries and the artery of Heubner.** In: Newton TH, Potts DG, eds. *Radiology of the skull and brain: angiography.* St. Louis: Mosby;1974;1527–1539
11. Kato Y, Nair S, Sano H, et al. **Multi-slice 3D-CTA: an improvement over single-slice helical CTA for cerebral aneurysms.** *Acta Neurochir (Wien)* 2002;144:715–722
12. Schueler BA, Sen A, Hsiung HH, Latchaw RE, Hu X. **Three-dimensional vascular reconstruction with a clinical X-ray angiography system.** *Acad Radiol* 1997;4:693–699